4554 *Biochemistry* **2010,** *49,* 4554–4563
DOI: 10.1021/bi1002822

BIOCHEMISTRY
including biophysical chemistry & molecular biology
Article

Monomorphic RNA G-Quadruplex and Polymorphic DNA G-Quadruplex Structures Responding to Cellular Environmental Factors[†]

Dong-Hao Zhang,[‡] Takeshi Fujimoto,[§] Sarika Saxena,[‡] Hai-Qing Yu,[‡] Daisuke Miyoshi,*[,‡,§] and Naoki Sugimoto*[,‡,§]

[‡]*Frontier Institute for Biomolecular Engineering Research* (*FIBER*) *and* [§]*Faculty of Frontiers of Innovative Research in Science and Technology* (*FIRST*)*, Konan University, 7-1-20 minatojima-minamimachi, Chuo-ku, Kobe 650-0047, Japan*

Received February 25, 2010; Revised Manuscript Received April 23, 2010

ABSTRACT: We systematically and quantitatively investigated the structure and thermodynamics of G-quadruplexes of RNAs and corresponding DNAs of the same sequences under molecular crowding conditions that mimic the high osmotic stress induced by the numerous molecules inside of living cells. Structural analyses demonstrated that various telomere RNA sequences folded into parallel-stranded G-quadruplexes in a manner independent of the surrounding conditions with different cations under both dilute and molecular crowding conditions. In contrast, DNA G-quadruplexes showed structural polymorphism. Moreover, we demonstrated that the G-quadruplexes of the RNA sequences were more stable than those of the same DNA sequences. These results show that a single and robust RNA G-quadruplex structure can exist in a manner independent of the sequence and surrounding conditions. To confirm this, we studied a guanine-rich sequence located in the 5′-untranslated region of human *bcl-2* mRNA that is thought to play a role in translation. The results revealed a stable parallel G-quadruplex that formed under all conditions tested. For example, a *bcl*-RNA G-quadruplex in the presence of 5 mM KCl [free energy change at 25 °C ($\Delta G°_{25}$) of −5.42 kcal/mol] was more stable than its corresponding DNA G-quadruplex ($\Delta G°_{25}$ = −2.31 kcal/mol). Our results further indicated that water molecules binding to the 2′-OH group of RNA G-quadruplexes play a critical role in their formation and stability.

Guanine-rich (G-rich)[1] sequences can fold into a G-quadruplex, a nucleic acid secondary structure consisting of stacked G-quartet planes connected by a network of Hoogsteen hydrogen bonds. DNA G-quadruplex structures are highly polymorphic, and a large number of structures have been observed (Figure 1) (*1*−*3*). The polymorphic structures of G-quadruplexes result in diverse functions, such as those observed in the human *c-kit* promoter, the *c-myc* promoter, and the thrombin-binding aptamer (*4*−*6*). Importantly, recent bioinformatic studies have revealed that not only DNA but also numerous mRNAs that contain G-rich sequences are able to fold into G-quadruplex structures (*7*−*10*), indicating that the RNA G-quadruplex is involved in the regulation of gene transcription and other biological processes. There have even been studies of the biological functions of such RNA G-quadruplexes. Balasubramanian and co-workers demonstrated for the first time that formation of a G-quadruplex in neuroblastoma RAS viral oncogene homologue (NRAS) 5′-untranslated region (UTR) mRNA has a critical function in its translation (*11*, *12*). Moreover, it has been reported that RNA G-quadruplexes found in the 5′-UTR of mRNAs are able to regulate protein synthesis inside various cells (*13*−*15*). Interestingly, recent analyses have identified a noncoding RNA containing the telomere sequence, $(uuag_3)_n$, that exists in the nuclear RNA fractions of human and mouse cells (*16*, *17*). In addition, Hartig and co-workers have reported that artificially introduced RNA G-rich sequences in mRNA regulate gene expression by folding into G-quadruplex structures (*18*, *19*). These reports clearly demonstrate the biological importance of RNA G-quadruplexes in vivo. However, biochemical and biophysical studies of G-quadruplexes to date have focused mainly on DNA, not RNA.

According to previous reports, different G-rich DNA sequences are able to fold into diverse G-quadruplex structures depending on various factors, including the loops and loop length, the flanking bases, and the G-tract length (*20*−*25*). Notably, not only the sequences but also the surrounding conditions determine the conformation of DNA G-quadruplexes. In particular, different monovalent and divalent cations coexisting in solution are known to induce diverse G-quadruplex structures with distinct thermodynamics (*26*−*30*). More importantly, it has been demonstrated that molecular crowding, the factor in the cellular environment with the greatest influence (*31*−*34*), induces polymorphic DNA G-quadruplexes and affects their stability (*35*−*38*). Therefore, to supplement the studies of the differences in the biochemical and biophysical properties of RNA and DNA G-quadruplexes (*39*−*44*), systematic and quantitative studies of the structures of G-rich RNA sequences under

[†]This work was supported in part by Grants-in-Aid for Scientific Research, the "Core Research" project (2009−2014), and the "Academic Frontier" project (2004−2009) from the Ministry of Education, Culture, Sports, Science and Technology, Japan; the Hirao Taro Foundation of the Konan University Association for Academic Research; and the Long-Range Research Initiative (LRI) Project of the Japan Chemical Industry Association.

*To whom correspondence should be addressed. D.M.: phone, +81-78-303-1426; fax, +81-78-303-1495; e-mail, miyoshi@center.konan-u.ac.jp. N.S.: phone, +81-78-303-1416; fax, +81-78-303-1495; e-mail, sugimoto@konan-u.ac.jp.

[1]Abbreviations: G-rich, guanine-rich; UTR, untranslated region; CD, circular dichroism; PAGE, polyacrylamide gel electrophoresis; UV, ultravisible; HPLC, high-performance liquid chromatography; PEG, poly(ethylene glycol); T_m, melting temperature; ORF, open reading frame; PDB, Protein Data Bank.

 Published on Web 04/27/2010

various conditions that induce molecular crowding are necessary. Such systematic studies may help elucidate the fundamental differences between noncanonical RNA and DNA structures.

In this study, the structure and stability of a series of G-rich RNA sequences and their corresponding DNA sequences were investigated by circular dichroism (CD), nondenaturing polyacrylamide gel electrophoresis (PAGE), and UV thermal denaturation measurements. The sequences include telomere sequences derived from various species and a sequence found in the mRNA of *bcl-2* (Table 1). Structural analyses showed that the G-rich RNA sequences were able to fold into only a parallel-stranded G-quadruplex, and that this folding was almost completely independent of sequence and surrounding factors such as monovalent cations and the concentration of cosolutes. In contrast, the structures of corresponding G-rich DNAs form various G-quadruplexes depended on the sequence and surrounding factors. Moreover, thermodynamic analyses of the RNA and DNA G-quadruplexes directly demonstrated that the parallel RNA G-quadruplex is more stable than parallel or antiparallel DNA G-quadruplexes under all conditions tested. Interestingly, the thermodynamic parameters of the RNA and DNA G-quadruplex formations indicate that differences in the molecular behavior of water during formation are induced by the 2′-OH groups of RNA and that these play a critical role in the higher stability of RNA G-quadruplexes. These chemical and energetic analyses can provide insights not only into structure-based drug design for targeting G-quadruplexes but also into how DNA and RNA G-quadruplexes have different biological roles in living cells.

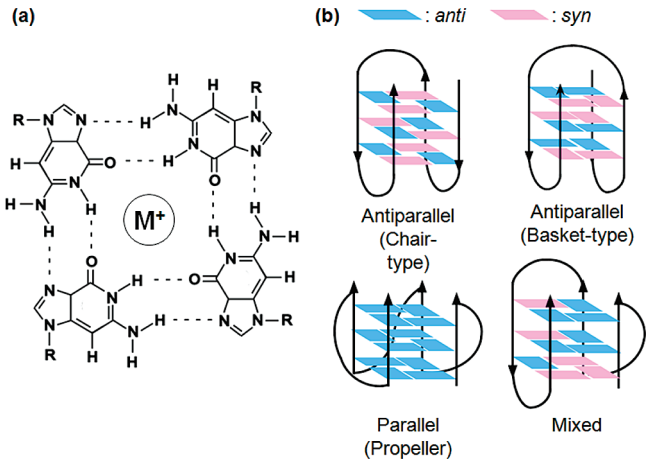

FIGURE 1: (a) Chemical structure of a G-quartet observed in a chair-type antiparallel G-quadruplex. A monovalent cation (M^+) occupies the central position. (b) Schematic representation of different structures of the intramolecular chair-type and basket-type antiparallel, parallel, and mixed G-quadruplexes.

MATERIALS AND METHODS

Materials. RNA and DNA strands used in this study were purchased from Hokkaido System Science Co., Ltd. (Hokkaido, Japan), and subsequently purified by high-performance liquid chromatography (HPLC). Single-strand concentrations of the RNA and DNA were determined by measurement of the absorbance at 260 nm at a high temperature using a Shimadzu (Kyoto, Japan) 1700 spectrophotometer connected to a thermoprogrammer. Single-strand extinction coefficients were calculated from mononucleotide and dinucleotide data using nearest-neighbor approximation (*45*). All other chemical reagents were reagent grade from Wako Pure Chemical Co., Ltd. (Osaka, Japan), and used without further purification.

CD Spectroscopy. CD spectra of RNA and DNA at a total strand concentration of 6 μM were recorded in a 0.1 cm pathlength quartz cell at 4 °C using a J-820 spectropolarimeter (Jasco Co., Ltd., Hachioji, Japan). The CD spectra were obtained by taking the average of three scans made at 0.5 nm intervals from 200 to 350 nm. Before CD measurements were taken, the samples were heated to 90 °C for 10 min, gently cooled at a rate of 0.2 °C/min, and incubated at 4 °C overnight. The temperature of the cell holder was regulated with a Jasco PTC-348 temperature controller, and the cuvette chamber was flushed with a constant stream of dry N_2 gas to prevent the condensation of water on the cuvette exterior.

Nondenaturing PAGE. Nondenaturing PAGE was conducted on 20% polyacrylamide (19:1 acrylamide/bisacrylamide) gels. Aliquots of 6 μM sample (3 μL each) were loaded and electrophoresed at 5 V/cm and 4 °C. Gels were stained using GelStar (Cambrex, Baltimore, MD) and visualized using an FLA-5100 imaging system (Fuji Film Co., Ltd., Tokyo, Japan). Before measurement, the samples were heated to 90 °C for 10 min, gently cooled at a rate of 0.2 °C/min, and incubated at 4 °C overnight.

Thermodynamic Analysis. The UV absorbance was measured with a Shimadzu 1700 spectrophotometer equipped with a temperature controller. Melting curves of G-quadruplexes were obtained by measurement of the UV absorbance at 295 nm in 30 mM Tris-HCl buffer (pH 7.0) containing 100 mM KCl or NaCl with various concentrations of poly(ethylene glycol) with an average molecular mass of 200 Da (PEG200). Before analysis, the samples were heated to 90 °C for 10 min, gently cooled at a rate of 0.2 °C/min, and incubated at 4 °C overnight. The heating rate was 0.5 °C/min, and the cuvette chamber was flushed with a constant stream of dry N_2 gas below 20 °C. Thermodynamic parameters, including melting temperatures (T_m), were calculated

Table 1: RNA and DNA Sequences Used in This Study[a]

abbreviation	sequence	sequence description
ht-RNA	5′-aggguuaggguuaggguuaggg-3′	human telomere
ht-DNA	5′-AGGGTTAGGGTTAGGGTTAGGG-3′	
tt-RNA	5′-gggguugggguugggguuuggg-3′	*Tetrahymena* telomere
tt-DNA	5′-GGGGTTGGGGTTGGGGTTGGGG-3′	
ot-RNA	5′-gggguuuugggguuuugggguuuuggggg-3′	*Oxytricha* telomere
ot-DNA	5′-GGGGTTTTGGGGTTTTGGGGTTTTGGGG-3′	
bcl-RNA	5′-gggccguggggugggagcuggg-3′	*bcl-2* gene
bcl-DNA	5′-GGGCCGTGGGGTGGGAGCTGGG-3′	

[a]Guanine stretches are underlined. RNA and DNA are depicted with lowercase and uppercase letters, respectively.

from the fit of the melting curves to a theoretical equation for intramolecular association as described previously (*38*). The thermodynamic parameters are the average values obtained from each melting curve with at least four different RNA or DNA strand concentrations.

Water Activity Measurements. Osmotic pressures were measured via vapor phase osmometry using the 5520XR pressure osmometer (Wescor). The water activity (a_w) was estimated from the measured osmolality (millimoles per kilogram) using eq 1 (*46*):

$$\psi = (RT/M_w) \ln a_w \quad (1)$$

where ψ and M_w represent the water potential and the molecular weight of water (0.018 kg/mol), respectively, R is the gas constant, and T is the temperature in kelvin. The relationship between water potential and osmolality, assuming independence of the water potential from temperature at room temperature, is given by eq 2 (*46*):

$$\psi \text{ (megapascals)} = \text{osmolality (millimoles per kilogram)} \times 10^3/(-400) \quad (2)$$

RESULTS

Sequence Design. The structures of RNA and DNA sequences derived from human telomere RNA (*ht*-RNA) and DNA (*ht*-DNA) (Table 1) were investigated because *ht*-DNA structure and stability have been well studied using various methods such as X-ray analysis, NMR, spectroscopic analysis, and molecular dynamics simulations (*3*, *26*−*30*). Moreover, Shafer and coworkers investigated the human telomere RNA G-quadruplex of $ag_3(u_2ag_3)_3$ (*ht*-RNA) in the presence of KCl and found that *ht*-RNA forms a parallel G-quadruplex that is different from that of *ht*-DNA (*39*). Recently, two groups (Xu and Komiyama, and Martadinata and Phan) independently demonstrated by NMR that RNA sequences similar to *ht*-RNA form a parallel G-quadruplex in the presence of Na^+ or K^+ (*47*, *48*). Therefore, RNA and DNA sequences derived from *ht*-RNA and *ht*-DNA should be optimal for investigating the similarity and dissimilarity in the structure and thermodynamic stability of RNA and DNA G-quadruplexes. The two other telomere sequences derived from *Tetrahymena* and *Oxytricha* (Table 1) were also investigated to confirm the properties of RNA and DNA G-quadruplexes. Notably, these telomere RNAs possess not only different sequences but also various G-tract lengths and loop contexts of different lengths. Therefore, it is possible to use these approaches to study the factors that govern the structure and stability of RNA G-quadruplexes. To validate the results from the telomere RNA G-quadruplexes, we also studied the B-cell CLL/lymphoma 2 (*bcl-2*) gene because its product, a mitochondrial membrane protein, is a key regulatory factor of programmed cell death (*49*). We found that the 5′-UTR of *bcl-2* mRNA included a G-rich sequence [5′-agggccgugggguggggagcuggg-3′ (*bcl*-RNA)] located adjacent to the open reading frame (ORF) (Figure 2). Interestingly, this sequence is strongly conserved in mice and humans (*50*), although its structure has not yet been studied. Since it has been proposed that the secondary structure of the mRNA around the ORF may be a promising target for the regulation of gene expression, it is important to study the structural formation of this G-rich RNA sequence as well as its corresponding DNA [5′-AGGGCCGTGGGGTGGGAGCTGGG-3′ (*bcl*-DNA)] sequence.

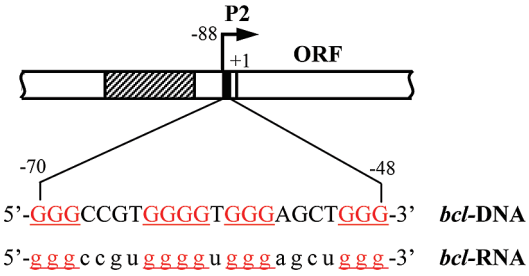

FIGURE 2: Schematic representation of the human *bcl-2* gene and the sequence of 5′-UTR DNA and the corresponding RNA. The hatched region represents introns. P2 located 88 bases upstream of the translation start site indicates the second promoter of the *bcl-2* gene, and ORF indicates the 5′-portion of the ORF. +1 indicates the translation start site. Guanine stretches located 48−70 bases upstream of the translation start site are underlined.

Structural Analysis of RNA Sequences and Their Corresponding DNA Sequences. It is well-known that an antiparallel G-quadruplex shows positive and negative peaks around 295 and 265 nm, respectively, while a parallel G-quadruplex shows positive and negative peaks around 260 and 240 nm, respectively (*36*). Moreover, a mixed parallel/antiparallel G-quadruplex shows positive peaks around 295 and 260 nm (*28*−*30*). Figure 3a shows the CD spectra of 6 μM *ht*-RNA in buffers containing 100 mM NaCl or KCl and 30 mM Tris-HCl (pH 7.0) with 0 or 40 wt % PEG200 at 4 °C. The CD spectrum in the presence of NaCl with PEG200 had large positive and negative peaks near 260 and 240 nm, respectively, which is characteristic of parallel G-quadruplexes (*36*). This suggests that *ht*-RNA forms a parallel G-quadruplex under these conditions. Similarly, the CD spectra of *ht*-RNA in the presence of KCl with or without PEG200 also exhibited the same positive and negative peaks, suggesting formation of the parallel G-quadruplex. Overall, these results indicate that *ht*-RNA has a stronger preference for the formation of the parallel G-quadruplex, which is consistent with previous structural studies of RNA G-quadruplexes (*47*, *48*). In addition, mixed G-quadruplexes of *ht*-RNA in the presence of NaCl are not consistent with NMR data (*47*), which instead show intramolecular and intermolecular parallel G-quadruplexes for *ht*-RNA sequences. However, the sequence used here, $a(ggguua)_3ggg$, was slightly different from those used in the NMR study, $(uuaggg)_4$ and uaggguuaggu. We confirmed that the sequence used in the NMR study showed typical CD spectra for the parallel G-quadruplex (Figure S1 of the Supporting Information). These results support the hypothesis that RNA sequences preferentially form parallel G-quadruplexes. Although the differences in the CD spectra imply that the flanking bases affect the whole structure of the telomere RNA sequences, further studies need to clarify this point.

In contrast with the corresponding RNA, the CD spectra of *ht*-DNA were strongly dependent on the conditions (Figure 3b). In the presence of NaCl without PEG200, the CD spectrum of *ht*-DNA showed positive and negative peaks around 295 and 265 nm, respectively, which is characteristic of antiparallel G-quadruplexes (*37*). In the presence of KCl without PEG200, the CD spectrum had positive peaks around both 295 and 260 nm, suggesting that the G-quadruplex had folded into a mixed G-quadruplex (*28*). In addition, in the presence of NaCl with PEG200, the CD spectrum indicated formation of an antiparallel G-quadruplex, but in the presence of KCl with PEG200, the G-quadruplex was parallel. These structural polymorphisms of *ht*-DNA are consistent with previous reports (*3*, *26*, *35*). Thus, in

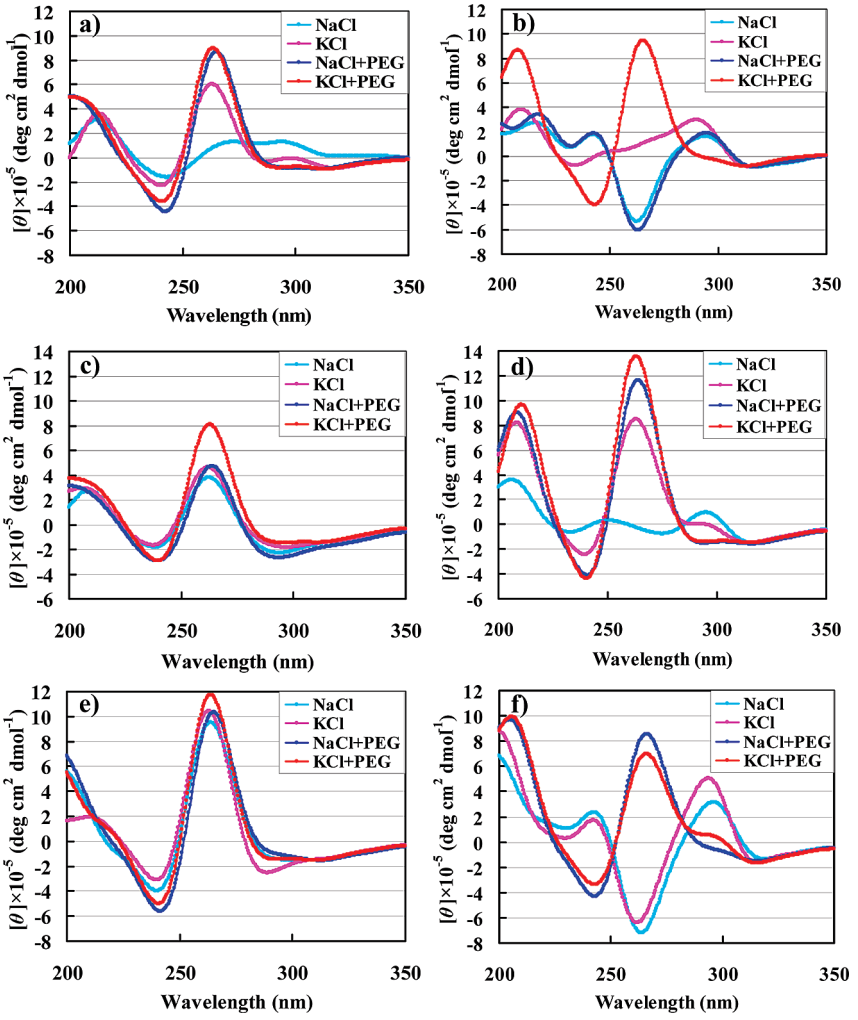

FIGURE 3: CD spectra of 6 μM (a) *ht*-RNA, (b) *ht*-DNA, (c) *tt*-RNA, (d) *tt*-DNA, (e) *ot*-RNA, and (f) *ot*-DNA in buffers containing 100 mM NaCl or KCl and 30 mM Tris-HCl (pH 7.0) with 0 or 40 wt % PEG200 at 4 °C. Bright blue, pink, dark blue, and red lines show CD spectra with 100 mM NaCl, 100 mM KCl, 100 mM NaCl and 40 wt % PEG200, and 100 mM KCl and 40 wt % PEG200, respectively.

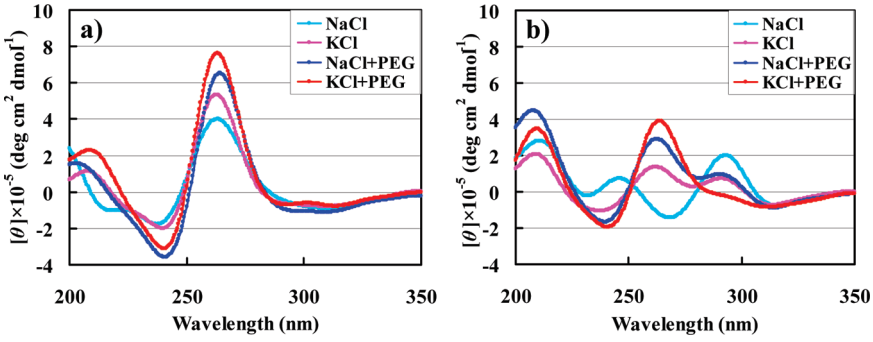

FIGURE 4: CD spectra of 6 μM (a) *bcl*-RNA and (b) *bcl*-DNA in buffers containing 100 mM NaCl or KCl and 30 mM Tris-HCl (pH 7.0) with 0 or 40 wt % PEG200 at 4 °C. Bright blue, pink, dark blue, and red lines show CD spectra with 100 mM NaCl, 100 mM KCl, 100 mM NaCl and 40 wt % PEG200, and 100 mM KCl and 40 wt % PEG200, respectively.

contrast with *ht*-RNA, *ht*-DNA forms various G-quadruplexes depending on the surrounding conditions.

The differences between RNA and DNA G-quadruplexes were further confirmed with *tt*-RNA and *tt*-DNA as well as *ot*-RNA and *ot*-DNA. Panels c and d of Figure 3 show the CD spectra of *tt*-RNA and *tt*-DNA, respectively, in buffers containing 100 mM NaCl or KCl and 30 mM Tris-HCl (pH 7.0) with 0 or 40 wt % PEG200 at 4 °C. The CD spectra of *tt*-RNA under all conditions tested showed that it folds into a parallel G-quadruplex, whereas *tt*-DNA folds into mixed or parallel G-quadruplexes depending on the conditions. These results are almost identical to the results for *ot*-RNA (Figure 3e) and *ot*-DNA (Figure 3f). Taking these results as well as previous studies for direct comparison of RNA and DNA G-quadruplexes of various sequences together (*40*, *44*), we are able to surmise that G-rich RNA sequences appear to fold into a single structure, that of a parallel G-quadruplex. Notably, this folding is almost completely independent of the surrounding conditions, even though telomere DNA sequences exhibited structural polymorphisms depending on the surrounding conditions. This different propensity of RNA and DNA

G-quadruplexes explains how RNA can maintain its biological functions inside living cells where various environmental factors are dynamically altered depending on the cell cycle and other biological processes.

Structure of bcl-RNA and bcl-DNA. To explore the concept described above for RNA and DNA G-quadruplex structures, two corresponding nucleotide sequences that have potential functions in vivo, *bcl*-RNA and *bcl*-DNA, were further investigated. Figure 4a shows the CD spectra of 6 μM *bcl*-RNA in buffers containing 100 mM NaCl or 100 mM KCl and 30 mM Tris-HCl (pH 7.0) with 0 or 40 wt % PEG200 at 4 °C. The CD spectra of *bcl*-RNA under all conditions had large positive and negative peaks near 260 and 240 nm, respectively, indicating a parallel G-quadruplex (*18*). This is in contrast to the results for *bcl*-DNA (Figure 4b). The CD spectrum of *bcl*-DNA suggested formation of an antiparallel G-quadruplex in the presence of NaCl without PEG200. On the other hand, in the presence of KCl without PEG200, the CD spectrum indicated a mixed G-quadruplex structure. In the presence of NaCl or KCl with PEG200, the predominant G-quadruplex was parallel, although the CD spectrum had a small shoulder near 295 nm. Thus, it is evident that the G-quadruplex of *bcl*-DNA undergoes a structural conversion from an antiparallel to parallel G-quadruplex because of molecular crowding by PEG200. These results for *bcl*-RNA and *bcl*-DNA are entirely consistent with the model derived from the telomere RNA and DNA sequences (Figure 3). Therefore, structural analyses in this study (*40*, *44*) and previous studies suggest that the monomorphic nature of RNA G-quadruplexes and the polymorphic nature of DNA G-quadruplexes may be one of the fundamental differences between how RNA and DNA function.

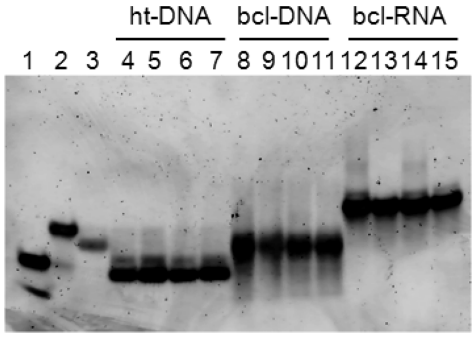

FIGURE 5: Nondenaturing 20% PAGE of *ht*-DNA, *bcl*-DNA, and *bcl*-RNA in the presence of 20 mM NaCl or KCl with 0 or 40 wt % PEG200 and 30 mM Tris-HCl (pH 7.0) at 4 °C: lane 1, Dickerson DNA duplex; lane 2, Dickerson RNA; lane 3, thrombin binding DNA aptamer forming the intermolecular antiparallel DNA G-quadruplex; lanes 4−7, G-quadruplex of *ht*-DNA with 20 mM NaCl, 20 mM KCl, 20 mM NaCl and 40 wt % PEG200, and 20 mM KCl and 40 wt % PEG200, respectively; lanes 8−11, G-quadruplex of *bcl*-DNA with 20 mM NaCl, 20 mM KCl, 20 mM NaCl and 40 wt % PEG200, and 20 mM KCl and 40 wt % PEG200, respectively; and lanes 12−15, *bcl*-RNA with 20 mM NaCl, 20 mM KCl, 20 mM NaCl and 40 wt % PEG200, and 20 mM KCl and 40 wt % PEG200, respectively. All measurements were taken with 3 μL of a 6 μM sample at 4 °C. Measurements for lanes 1−3 were taken in the buffer containing 20 mM NaCl and 30 mM Tris-HCl (pH 7.0).

We further investigated the structures of *bcl*-RNA and *bcl*-DNA using nondenaturing PAGE. Figure 5 shows the migration of the Dickerson dodecamer duplex of DNA (*51*) and its corresponding RNA (lanes 1 and 2, respectively), the thrombin binding DNA aptamer forming a unimolecular G-quadruplex (lane 3), *ht*-DNA (lanes 4−7), *bcl*-DNA (lanes 8−11), and *bcl*-RNA (lanes 12−15) in the presence of 20 mM NaCl or KCl with 0 or 40 wt % PEG200 at 4 °C. We found that the Dickerson DNA migrated faster than the corresponding RNA. This may because of differences in the structures of DNA and RNA duplexes. Since it has been reported that the thrombin binding DNA aptamer and *ht*-DNA fold into unimolecular structures (*38*, *39*, *42*, *43*), these bands can be markers for the migration of the unimolecular G-quadruplex of DNA. *bcl*-DNA comigrated with the *ht*-DNA G-quadruplex, indicating a unimolecular G-quadruplex for *bcl*-DNA. Moreover, *bcl*-RNA migrated slower than *bcl*-DNA. According to the difference in the migrations of the Dickerson RNA and DNA, it is reasonable to conclude that *bcl*-RNA forms a unimolecular G-quadruplex under these conditions. The unimolecular structure of *bcl*-RNA will be discussed later with its thermodynamic data. It should be stated that, in the case of *bcl*-DNA, PAGE showed the same band under various conditions in spite of the fact that the G-quadruplex structure of *bcl*-DNA was different depending on the surrounding conditions. This suggests that different G-quadruplex structures, such as parallel or antiparallel, could not be distinguished by PAGE.

Thermodynamic Analysis of bcl-RNA and bcl-DNA. Although G-rich RNA sequences formed parallel G-quadruplexes, the molecularity of their formation remained unclear. Thus, we further investigated the thermodynamics of the parallel G-quadruplex of *bcl*-RNA. Figure 6a shows normalized annealing and melting UV profiles of 6 μM *bcl*-RNA at 295 nm in 30 mM Tris-HCl (pH 7.0) containing 5 mM KCl. We chose this salt concentration because the G-quadruplex of *bcl*-RNA in the presence of 100 mM KCl is too stable to be analyzed thermodynamically. There was no hysteresis in the melting and annealing

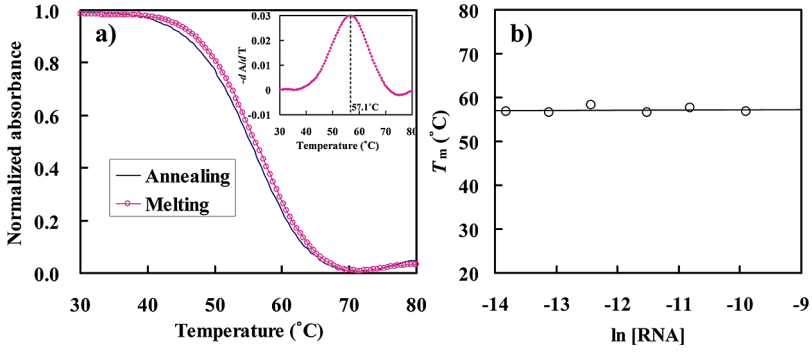

FIGURE 6: (a) Normalized melting and annealing UV profiles at 295 nm of *bcl*-RNA at a strand concentration of 6 μM in 30 mM Tris-HCl (pH 7.0) containing 5 mM KCl. The inset shows the first derivative of the melting curve. (b) Plot of T_m values vs log *bcl*-RNA strand concentration (1−50 μM) in 30 mM Tris-HCl (pH 7.0) containing 5 mM KCl.

curves. We evaluated the values of T_m by curve fitting, and the T_m values in the melting and annealing curves were almost identical (~57 °C). These results show that the folding and unfolding of the G-quadruplex of *bcl*-RNA occur via a two-state transition (*42*), allowing us to evaluate the thermodynamic parameters of the parallel RNA G-quadruplex. Furthermore, evaluation of T_m values with different concentrations of *bcl*-RNA using the melting curves showed constant values for the G-quadruplex of *bcl*-RNA at all RNA concentrations tested (Figure 6b), consistent with the formation of the intramolecular G-quadruplex observed in nondenaturing PAGE (Figure 5).

Since potassium is the dominant monovalent cation inside cells, we studied the thermal stability of the G-quadruplexes of both *bcl*-RNA and *bcl*-DNA in the presence of various concentrations of KCl (Figure S2a,b of the Supporting Information). Figure 7 shows T_m values for the G-quadruplexes of *bcl*-RNA and *bcl*-DNA in the presence of various concentrations of KCl. Interestingly, the T_m value of the RNA G-quadruplex is much higher than that of the corresponding DNA G-quadruplex at the same concentration of KCl. A higher stability of the RNA G-quadruplex was also observed in *ht*-RNA and *ht*-DNA (Figure S3 of the Supporting Information), in *tt*-RNA and *tt*-DNA (Figure S4 of the Supporting Information), and in *ot*-RNA and *ot*-DNA (Figure S5 of the Supporting Information). In addition to previous studies indicating that an RNA G-quadruplex is more stable than a corresponding DNA G-quadruplex (*40*−*44*, *52*), these results provide evidence that parallel RNA G-quadruplexes are generally more stable than any parallel, antiparallel, or mixed DNA G-quadruplexes.

Next, we studied the effect of molecular crowding on the thermodynamics of RNA G-quadruplexes. Figure 8a shows UV melting curves of the G-quadruplex of *bcl*-RNA in the presence of 5 mM KCl with 0, 10, 20, 30, or 40 wt % PEG200. The T_m value of the G-quadruplex of *bcl*-RNA increased from 58.0 to 77.7 °C as the PEG200 concentration increased from 0 to 40 wt %, demonstrating that the RNA G-quadruplex was stabilized by the molecular crowding of PEG200. In the same way, the T_m of the G-quadruplex of *bcl*-DNA increased from 42.6 to 68.5 °C (Figure 8b). Although the G-quadruplex of *bcl*-DNA underwent a structural transition from the mixed parallel/antiparallel G-quadruplex to a sole parallel G-quadruplex when the PEG200 concentration increased from 0 to 10 wt % (Figure S6 of the Supporting Information), melting curves of the mixed and parallel G-quadruplexes with a single transition indicated that these quadruplexes possess similar stability. Thus, it is possible to compare the stabilities of RNA and DNA G-quadruplexes using various concentrations of PEG200. Similar to the results in the dilute solution, the DNA G-quadruplex was less stable than the RNA G-quadruplex at the same concentrations of PEG200 which is consistent with the previous report for the human telomere RNA and DNA sequences (*44*).

To assess the origin of the observed stabilities of G-quadruplexes of *bcl*-RNA and *bcl*-DNA, the thermodynamic parameters of their formations, such as the enthalpy change ($\Delta H°$), entropy change ($\Delta S°$), and free energy change at 25 °C ($\Delta G°_{25}$), were estimated in the presence of various concentrations of PEG200 (Table 2). With a PEG200 concentration increasing from 0 to 40 wt % in a buffer containing 5 mM KCl and 30 mM Tris-HCl (pH 7.0), $\Delta H°$ decreased from −54.0 to −60.6 kcal/mol, $T\Delta S°$ decreased from −48.6 to −51.6 kcal/mol, and $\Delta G°_{25}$ decreased from −5.42 to −9.00 kcal/mol for the formation of the G-quadruplex of *bcl*-RNA. Therefore, stabilization of the RNA G-quadruplex by PEG200 is promoted by a favorable enthalpic contribution exceeding the unfavorable entropy change. Enthalpic stabilization of the G-quadruplex by molecular crowding has also been reported for DNA and RNA G-quadruplexes (*38*, *42*−*44*).

Although the structure of *bcl*-DNA at various concentrations of PEG200 is a mixture of antiparallel and parallel G-quadruplexes, UV melting curves with various concentrations of PEG200 show only a single transition (Figure 8b), indicating similar stabilities of the antiparallel and parallel G-quadruplexes. Thus, the thermodynamic parameters of *bcl*-DNA were evaluated with the assumption of formation of a two-state structure (Table 2). The enthalpic stabilization of the G-quadruplex was also observed in *bcl*-DNA.

Dehydration upon Formation of G-Quadruplex bcl-RNA and bcl-DNA. Since hydration is important for understanding

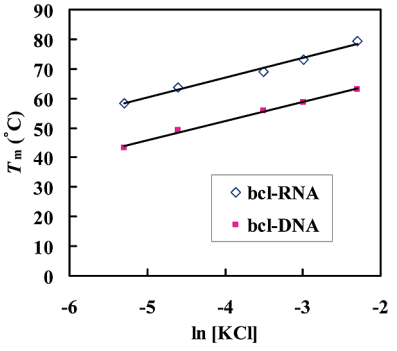

FIGURE 7: Comparison of T_m values at a strand concentration of 4 μM of *bcl*-RNA and *bcl*-DNA at different KCl concentrations in 30 mM Tris-HCl (pH 7.0).

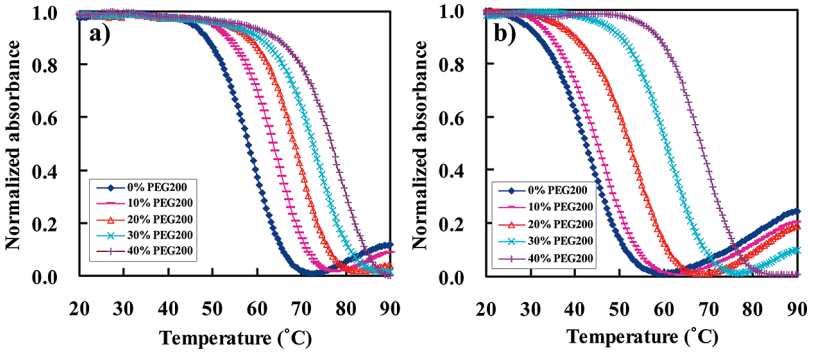

FIGURE 8: Normalized UV melting curves at 295 nm for 4 μM (a) *bcl*-RNA and (b) *bcl*-DNA in 30 mM Tris-HCl (pH 7.0) containing 5 mM KCl and 0, 10, 20, 30, or 40 wt % PEG200.

Table 2: Thermodynamic Parameters for Formation of a G-Quadruplex of *bcl*-RNA and *bcl*-DNA and Water Activity at Different PEG200 Concentrations (weight percent)[a]

	PEG200 (wt %)	$\Delta H°$ (kcal/mol)	$T\Delta S°$ (kcal/mol)	$\Delta G°_{25}$ (kcal/mol)	T_m[b] (°C)	ln a_w ($\times 10^{-2}$)
bcl-RNA	0	−54.0 ± 0.5	−48.6 ± 0.7	−5.42 ± 0.1	58.0	−0.08
	10	−55.4 ± 0.9	−49.0 ± 0.8	−6.40 ± 0.2	63.9	−1.00
	20	−56.9 ± 1.7	−49.6 ± 1.3	−7.28 ± 0.3	68.7	−2.28
	30	−59.5 ± 1.5	−51.2 ± 1.1	−8.28 ± 0.2	73.2	−3.98
	40	−60.6 ± 1.6	−51.6 ± 1.4	−9.00 ± 0.3	77.7	−4.65
bcl-DNA	0	−41.4 ± 0.7	−39.1 ± 0.8	−2.31 ± 0.1	42.6	−0.08
	10	−42.2 ± 0.6	−39.5 ± 0.5	−2.68 ± 0.1	45.2	−1.00
	20	−43.0 ± 0.7	−39.4 ± 1.0	−3.66 ± 0.2	52.7	−2.28
	30	−50.8 ± 1.6	−45.4 ± 1.3	−5.46 ± 0.2	60.9	−3.98
	40	−53.5 ± 1.9	−46.7 ± 1.8	−6.81 ± 0.3	68.5	−4.65

[a]The buffer was 5 mM KCl in 30 mM Tris-HCl (pH 7.0). [b]The melting temperature was determined at a strand concentration of 4 μM.

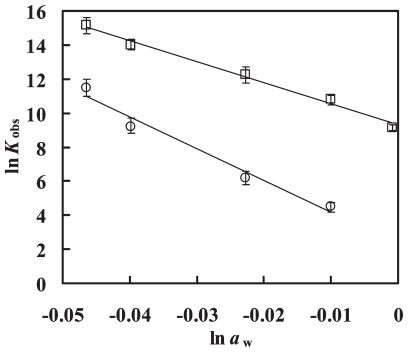

FIGURE 9: Plots of ln K_{obs} vs ln a_w for formation of the G-quadruplex of *bcl*-RNA (□) and *bcl*-DNA (○) in 30 mM Tris-HCl (pH 7.0) containing 5 mM KCl and 10, 20, 30, or 40 wt % PEG200 at 25 °C. The error bars were calculated using at least three different RNA or DNA strand concentrations.

the structure and stability of G-quadruplexes (*38*), we investigated the behavior of water molecules during the formation of RNA and DNA G-quadruplexes. The formation of an intramolecular structure by oligonucleotides in an aqueous solution containing a cosolute and a cation (K^+) can be represented as follows (*38*, *53*):

$$A_{SS} \rightleftarrows A_f + \Delta n_w H_2O + \Delta n_{CS} CS + \Delta n_{M^+} M^+ \quad (3)$$

where A_{SS} and A_f represent single-stranded and folded DNA or RNA structures, respectively, CS is the cosolute, M^+ is a cation, and Δn_w, Δn_{CS}, and Δn_{M^+} are the respective numbers of water molecules, cosolute molecules, and cations released upon formation of the structure, respectively. The observed equilibrium constant (K_{obs}) for the formation of the structure at constant temperature and pressure is thus given as

$$\frac{d(\ln K_{obs})}{d(\ln a_w)} = -\left\{\Delta n_w + \Delta n_{CS}\left[\frac{d(\ln a_{CS})}{d(\ln a_w)}\right] + \Delta n_{M^+}\left[\frac{d(\ln a_{M^+})}{d(\ln a_w)}\right]\right\} \quad (4)$$

where a_w, a_{CS}, and a_{M^+} are the activities of water, cosolute, and cation, respectively.

Figure 9 shows plots of ln K_{obs} for the formation of the G-quadruplex of *bcl*-RNA and *bcl*-DNA versus ln a_w at 25 °C. The stability (ln K_{obs}) of the G-quadruplex decreased linearly with the increase in water activity (ln a_w). The slope ($-\Delta n_w$) of the ln K_{obs} versus ln a_w plot for the G-quadruplex of *bcl*-RNA in the presence of KCl was estimated to be −124, indicating that 5.6 water molecules per nucleotide on average were released upon formation of the parallel G-quadruplex of *bcl*-RNA. Since the parallel G-quadruplex of *bcl*-DNA becomes the dominant structure in 10−40 wt % PEG200 (Figure S6 of the Supporting Information), we further evaluated the number of released water molecules with the four data points at 10, 20, 30, and 40 wt % PEG200. The slope of the plot of ln K_{obs} for the formation of the parallel G-quadruplex of *bcl*-DNA versus ln a_w was −186, indicating that 8.5 water molecules per nucleotide were released on average upon formation of the parallel G-quadruplex of *bcl*-DNA. This number was 2.9 more than that of *bcl*-RNA. The number of water molecules released upon the formation of human telomere RNA was evaluated to be 6.0 (*44*). This number was 2.0 more than that of the corresponding DNA (*44*). The concentration of K^+ in their study is 100 mM, which is much higher than that in this study (5 mM). This difference can affect the hydration state of the G-quadruplex because dehydration of the cation also contributes to the total number of water molecules released through formation of the G-quadruplex (*38*). These results suggest that the 2′-OH group in the RNA sugar ring as well as the methyl group in dT, the difference distinguishing ribonucleosides from deoxyribonucleosides, may play a role in the behavior of water molecules, as we will discuss later.

DISCUSSION

G-Quadruplexes are generally folded into one of three principal topologies, antiparallel, parallel, or mixed (Figure 1). In the antiparallel and mixed topologies, half of the guanine nucleotides possesses the *anti* conformation in the glycosidic bond and the other half possesses the *syn* conformation. On the other hand, all guanine nucleotides adopt the *anti* conformation in the parallel topology. A previous study of RNA and DNA duplexes demonstrated more difficulty in inducing the Z-form duplex with poly(rG-rC)·poly(rG-rC) than with poly(dG-dC)·poly(dG-dC) (*54*). It was also proposed in the same study that the higher energy of the *syn* conformation in the RNA duplex versus that in the DNA duplex inhibits formation of the Z-form RNA duplex (*54*). These results demonstrated that a ribonucleotide has a stronger propensity than a deoxyribonucleotide to adopt the *anti* conformation in a duplex. This difference is due to the ribose 2′-hydroxyl group. A molecular dynamics simulation (*55*) and a study of RNA duplex hydration (*56*) showed that the 2′-OH group alters the sugar pucker and mediates 3′−5′ intrastrand O2′···O4′ hydrogen bonding. The sugar pucker is coupled to the glycosidic torsion angle and the *syn*−*anti* properties of the nucleoside. The 2′-position of the sugar moiety is important not only for duplex formation but also for G-quadruplex formation.

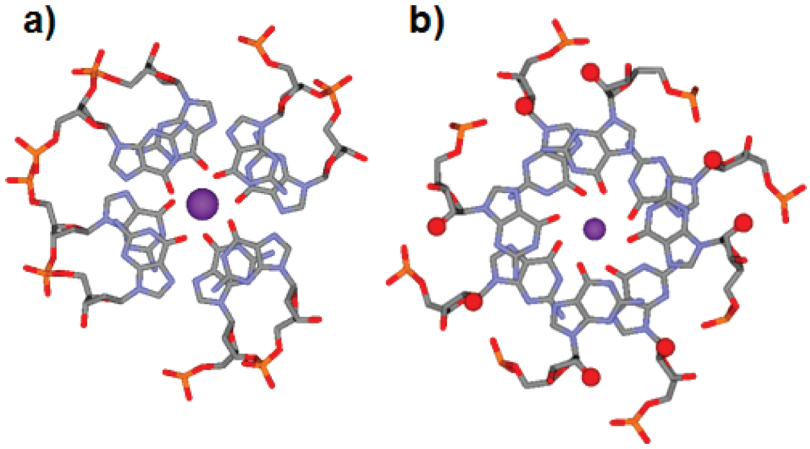

FIGURE 10: Two G-quartet planes in an antiparallel DNA G-quadruplex (a) and in a parallel RNA G-quadruplex (b). The structures were generated with the crystal structures of d(GGGGTTTTGGGG) (PDB entry 1JPQ) and r(UGGUGU) (PDB entry 2AWE) for the DNA G-quadruplex and RNA G-quadruplex, respectively. The 2′-OH groups in RNA are highlighted as red spheres. The centers of the G-quartets are depicted as purple spheres.

Mergny and co-workers found that substitution of the ribose 2′-OH group with a methoxy group changes the G-quadruplex structure (*52*). These results demonstrate the importance of the 2′-OH group for the whole G-quadruplex structure. From these considerations, the stronger propensity of riboguanosine for the *anti* conformation may be the reason that RNA forms only a single parallel G-quadruplex structure regardless of the surrounding conditions. Therefore, the structural data obtained in this study are important systematic and comparative results directly showing the differences between RNA and DNA structures.

The thermodynamic parameters obtained in this study show that the RNA G-quadruplex is more thermodynamically stable than the DNA G-quadruplex, although sometimes their structures are different. It has been reported that the parallel G-quadruplex of $d(G_4T_4G_4)$ induced by molecular crowding is more stable than the antiparallel G-quadruplex that forms under dilute conditions (*37*). However, in that study, conditions such as coexisting cations and solutes that induce parallel and antiparallel G-quadruplexes were very different, even though the sequences were the same. On the other hand, we found that both *bcl*-RNA and *bcl*-DNA formed parallel G-quadruplexes under identical conditions [5 mM KCl with 40 wt % PEG200 (Figure 4)] and the G-quadruplex of *bcl*-RNA was more stable than that of *bcl*-DNA (Figure 8). In addition, the parallel G-quadruplex of *tt*-RNA in the presence of KCl without PEG200 was more stable than the parallel G-quadruplex of *tt*-DNA under the same conditions (Figure 3c,d and Figure S4 of the Supporting Information). Therefore, the higher stability of the RNA G-quadruplex is due to the different properties of RNA and DNA but not to differences in strand orientation such as their parallel or antiparallel topologies.

This difference in the stabilities of RNA and DNA G-quadruplexes can be attributed to the 2′-OH group. The quantitative results for hydration of the G-quadruplexes of *bcl*-RNA and *bcl*-DNA obtained in this study revealed a critical role of the 2′-OH moiety in the higher stability seen in the RNA G-quadruplex. Since the O−H···O hydrogen bond is a strongly directional interaction, the presence of the 2′-OH group not only brings in water molecules but also provides a set of strongly directional arms on which to build the rest of the water molecule framework. Therefore, the 2′-OH group can affect the water molecules bound to the G-quadruplex. Panels a and b of Figure 10 show two G-quartet planes in an antiparallel DNA G-quadruplex and a parallel RNA G-quadruplex, respectively. The structures are based on the crystal structures of the antiparallel DNA G-quadruplex (PDB entry 1JPQ) and parallel RNA G-quadruplex (PDB entry 2AWE) in the presence of K^+ (*57*, *58*). Dehydration of the guanine bases and cations upon formation of a G-quadruplex is common for RNA and DNA which has been shown in previous studies (*38*, *42*, *44*). However, hydration at the grooves of the G-quadruplex should be different between RNA and DNA because the ordered 2′-OH groups at the groove of the RNA G-quadruplex (highlighted as red circles in Figure 10b) are favored to take up water molecules. In a study of RNA duplexes, Egli and co-workers provided evidence of an important role of the 2′-OH group in the thermodynamics of an RNA duplex (*56*). They showed that the presence of the additional hydroxyl group in the sugar moiety not only confers more water onto the RNA backbone portion but also leads overall to a more ordered water structure at the grooves (*56*). Moreover, molecular dynamics simulations have shown that the 2′-OH group locks the sugar pucker, resulting in RNA helices that are less mobile than DNA helices (*55*). This is consistent with the numbers of water molecules released during formation of *bcl*-RNA and *bcl*-DNA G-quadruplexes (Figure 9) and thermodynamic parameters (Table 2). The number of water molecules released per nucleotide during formation of the RNA and DNA G-quadruplexes was estimated to be 5.6 and 8.5, respectively. Therefore, the 2′-OH group, as well as the difference between dT and rU (*43*), plays a role as a scaffold that can take up 2.9 ($=8.5-5.6$) water molecules per nucleotide. This difference in the number of water molecules stabilizes the RNA G-quadruplex with an enthalpic contribution. This enthalpic contribution was also observed in previous studies of hydration of DNA and RNA G-quadruplexes (*38*, *42*−*44*). In addition, we further attempted to evaluate the thermodynamic parameters and number of water molecules released during formation of the G-quadruplex of *ot*-RNA, *ot*-DNA, *tt*-RNA, and *tt*-DNA. However, we found hysteresis between the melting and annealing curves for *ot*-RNA and *ot*-DNA (Figure S7a,b of the Supporting Information), indicating a non-two-state transition. On the other hand, hysteresis was not observed in the case of *tt*-RNA and *tt*-DNA (Figure S7c,d of the Supporting Information). Although it was difficult to evaluate accurate $\Delta H°$ and $\Delta S°$ values because of the high T_m values as shown in panels a and b of Figure S8 of the Supporting Information, it was possible to

evaluate the ΔG° value, corresponding to ln K_{obs}. The numbers of water molecules released through the formation of G-quadruplexes of *tt*-RNA and *tt*-DNA (Figure S8c of the Supporting Information) were determined to be 4.6 and 7.9, respectively, per nucleotide. These values also support the hypothesis mentioned above. These results led to the conclusion that the higher stability of the RNA G-quadruplex arises from the 2′-OH group in RNA acting as a scaffold for a water network at the grooves and thus stabilizing the sugar pucker and locking the sugar−phosphate backbone in the *anti* conformation, resulting in a single and robust RNA G-quadruplex.

BIOLOGICAL SIGNIFICANCE AND CONCLUSIONS

In addition to NMR and X-ray crystallographic studies, it is widely held that biochemical and biophysical studies of nucleic acids under molecular crowding conditions are necessary to understand their intracellular properties. The results of this study confirmed that the RNA G-quadruplex structure revealed by NMR was maintained even under molecular crowding conditions because of the restriction in the glycosidic torsion angle. Moreover, distinct structural forms of biomolecules implicate distinct biological functions. In particular, a single and robust nucleic acid structure provides a more advantageous platform than a polymorphic nucleic acid structure for high-specificity protein binding or for the design of small molecules to target nucleic acids. One has to take the surrounding conditions into consideration when developing ligands and drugs targeting nucleic acids if their structures are condition-dependent. In fact, osmotic pressure, a physical parameter related to water activity that is a measure of intracellular crowding, is altered significantly during the cell cycle (*31*). In this study, we found that G-rich RNA sequences predominantly fold into stable parallel G-quadruplexes regardless of the surrounding conditions. In contrast, DNA G-quadruplexes are structures that adopt polymorphic topologies depending on surrounding conditions such as coexisting cations and cosolutes at various concentrations. Therefore, the structure and thermodynamics of a DNA G-quadruplex may change depending on cell conditions. However, the RNA G-quadruplex is the sole structure that forms, and this structure is unaffected by the surrounding conditions. This dissimilarity is a fundamental difference between noncanonical DNA and RNA structures. Moreover, understanding the monomorphic and stable G-quadruplex structure of mRNAs and the G-rich RNAs studied here may lead to new approaches for cancer therapy at the translational level, which is distinct from traditional cancer therapeutic interventions that target transcription.

SUPPORTING INFORMATION AVAILABLE

Normalized UV melting curves of the G-quadruplexes of *bcl*-RNA and *bcl*-DNA with various concentrations of KCl; normalized UV melting curves of the G-quadruplexes of *ht*-RNA and *ht*-DNA, *tt*-RNA and *tt*-DNA, and *ot*-RNA and *ot*-DNA with various concentrations of KCl; CD spectra of *bcl*-DNA with different concentrations of PEG200; normalized UV melting and annealing curves of the G-quadruplexes of *ot*-RNA, *ot*-DNA, *tt*-RNA, and *tt*-DNA in the presence of 1 mM KCl; normalized UV melting curves of the G-quadruplexes of *tt*-RNA and *tt*-DNA with various concentrations of PEG200; and plot of ln K_{obs} versus ln a_w. This material is available free of charge via the Internet at http://pubs.acs.org.

REFERENCES

1. Simonsson, T. (2001) G-quadruplex DNA structures variations on a theme. *Biol. Chem. 382*, 621–628.
2. Williamson, J. R. (1994) G-quartet structures in telomeric DNA. *Annu. Rev. Biophys. Biomol. Struct. 23*, 703–730.
3. Parkinson, G. N., Lee, M. P. H., and Neidle, S. (2002) Crystal structure of parallel quadruplexes from human telomeric DNA. *Nature 417*, 876–880.
4. Phan, A. T., Kuryavyi, V., Burge, S., Neidle, S., and Patel, D. J. (2007) Structure of an unprecedented G-quadruplex scaffold in the human *c-kit* promoter. *J. Am. Chem. Soc. 129*, 4386–4392.
5. Seenisamy, J., Rezler, E. M., Powell, T. J., Tye, D., Gokhale, V., Joshi, C. S., Siddiqui-Jain, A., and Hurley, L. H. (2004) The dynamic character of the G-quadruplex element in the c-MYC promoter and modification by TMPyP4. *J. Am. Chem. Soc. 126*, 8702–8709.
6. Tang, C.-F., and Shafer, R. H. (2006) Engineering the quadruplex fold: Nucleoside conformation determines both folding topology and molecularity in guanine quadruplexes. *J. Am. Chem. Soc. 128*, 5966–5973.
7. Hazel, P., Parkinson, G. N., and Neidle, S. (2006) Predictive modelling of topology and loop variations in dimeric DNA quadruplex structures. *Nucleic Acids Res. 34*, 2117–2127.
8. Kikin, O., D'Antonio, L., and Bagga, P. S. (2006) QGRS mapper: A web-based server for predicting G-quadruplexes in nucleotide sequences. *Nucleic Acids Res. 34*, w676–w682.
9. Zanotti, K. J., Lackey, P. E., Evans, G. L., and Mihailescu, M.-R. (2006) Thermodynamics of the fragile X mental retardation protein RGG box interactions with G-quartet forming RNA. *Biochemistry 45*, 8319–8330.
10. Huppert, J. L., Bugaut, A., Kumari, S., and Balasubramanian, S. (2008) G-quadruplexes: The beginning and end of UTRs. *Nucleic Acids Res. 36*, 6260–6268.
11. Kumari, S., Bugaut, A., Huppert, J. L., and Balasubramanian, S. (2007) An RNA G-quadruplex in the 5′-UTR of the NRAS proto-oncogene modulates translation. *Nat. Chem. Biol. 3*, 218–221.
12. Kumari, S., Bugaut, A., and Balasubramanian, S. (2008) Position and stability are determining factors for translation repression by an RNA G-quadruplex-forming sequence within the 5′ UTR of the NRAS proto-oncogene. *Biochemistry 47*, 12664–12669.
13. Arora, A., Dutkiewicz, M., Scaria, V., Hariharan, M., Maiti, S., and Kurreck, J. (2008) Inhibition of translation in living eukaryotic cells by an RNA G-quadruplex motif. *RNA 14*, 1290–1296.
14. Balkwill, G. D., Derecka, K., Garner, T. P., Hodgman, C., Flint, A. P., and Searle, M. S. (2009) Repression of translation of human estrogen receptor α by G-quadruplex formation. *Biochemistry 48*, 11487–11495.
15. Morris, M. J., and Basu, S. (2009) An unusually stable G-quadruplex within the 5′-UTR of the MT3 matrix metalloproteinase mRNA represses translation in eukaryote cells. *Biochemistry 48*, 5313–5319.
16. Azzalin, C. M., Reichenbach, P., Khoriauli, L., Giulotto, E., and Lingner, J. (2007) Telomeric repeat-containing RNA and RNA surveillance factors at mammalian chromosome ends. *Science 318*, 798–801.
17. Schoeftner, S., and Blasco, M. A. (2008) Developmentally regulated transcription of mammalian telomeres by DNA-dependent RNA polymerase II. *Nat. Cell Biol. 10*, 228–236.
18. Wieland, M., and Hartig, J. S. (2007) RNA quadruplex-based modulation of gene expression. *Chem. Biol. 14*, 757–763.
19. Halder, K., Wieland, M., and Hartig, J. S. (2009) Predictable suppression of gene expression by 5′-UTR-based RNA quadruplexes. *Nucleic Acids Res. 37*, 6811–6817.
20. Hazel, P., Huppert, J., Balasubramanian, S., and Neidle, S. (2004) Loop-length-dependent folding of G-quadruplexes. *J. Am. Chem. Soc. 126*, 16405–16415.
21. Risitano, A., and Fox, K. R. (2004) Influence of loop size on the stability of intramolecular DNA quadruplexes. *Nucleic Acids Res. 32*, 2598–2606.
22. Rachwal, P. A., Findlow, I. S., Werner, J. M., Brown, T., and Fox, K. R. (2007) Intramolecular DNA quadruplexes with different arrangements of short and long loops. *Nucleic Acids Res. 35*, 4214–4222.
23. Antonacci, C., Chaires, J. B., and Sheardy, R. D. (2007) Biophysical characterization of the human telomeric $(TTAGGG)_4$ repeat in a potassium solution. *Biochemistry 46*, 4654–4660.
24. Guo, Q., Lu, M., and Kallenbach, N. R. (1993) Effect of thymine tract length on the structure and stability of model telomeric sequences. *Biochemistry 32*, 3596–3603.
25. Rachwal, P. A., Brown, T., and Fox, K. R. (2007) Effect of G-tract length on the topology and stability of intramolecular DNA quadruplexes. *Biochemistry 46*, 3036–3044.

26. Wang, Y., and Patel, D. J. (1993) Solution structure of the human telomeric repeat d[$AG_3(T_2AG_3)_3$] G-tetraplex. *Structure 1*, 263–282.
27. Miyoshi, D., Nakao, A., and Sugimoto, N. (2003) Structural transition from antiparallel to parallel G-quadruplex of d($G_4T_4G_4$) induced by Ca^{2+}. *Nucleic Acids Res. 31*, 1156–1163.
28. Xu, Y., Noguchi, Y., and Sugiyama, H. (2006) The new models of the human telomere d[$AGGG(TTAGGG)_3$] in K^+ solution. *Bioorg. Med. Chem. 14*, 5584–5591.
29. Ambrus, A., Chen, D., Dai, J., Bialis, T., Jones, R. A., and Yang, D. (2006) Human telomeric sequence forms a hybrid-type intramolecular G-quadruplex structure with mixed parallel/antiparallel strands in potassium solution. *Nucleic Acids Res. 34*, 2723–2735.
30. Phan, A. T., Luu, K. N., and Patel, D. J. (2006) Different loop arrangements of intramolecular human telomeric (3+1) G-quadruplexes in K^+ solution. *Nucleic Acids Res. 34*, 5715–5719.
31. Zimmerman, S. B., and Minton, A. P. (1993) Macromolecular crowding: Biochemical, biophysical, and physiological consequences. *Annu. Rev. Biophys. Biomol. Struct. 22*, 27–65.
32. Minton, A. P. (2001) The influence of macromolecular crowding and macromolecular confinement on biochemical reactions in physiological media. *J. Biol. Chem. 276*, 10577–10580.
33. Morar, A. S., and Pielak, G. J. (2002) Crowding by trisaccharides and the 2:1 cytochrome c-cytochrome c peroxidase complex. *Biochemistry 41*, 547–551.
34. Miyoshi, D., and Sugimoto, N. (2008) Molecular crowding effects on structure and stability of DNA. *Biochimie 9*, 1040–1051.
35. Li, J., Correia, J. J., Wang, L., Trent, J. O., and Chaires, J. B. (2005) Not so crystal clear: The structure of the human telomere G-quadruplex in solution differs from that present in a crystal. *Nucleic Acids Res. 33*, 4649–4659.
36. Miyoshi, D., Matsumura, S., Nakano, S., and Sugimoto, N. (2004) Duplex dissociation of telomere DNAs induced by molecular crowding. *J. Am. Chem. Soc. 126*, 165–169.
37. Miyoshi, D., Nakao, A., and Sugimoto, N. (2002) Molecular crowding regulates the structural switch of the DNA G-quadruplex. *Biochemistry 41*, 15017–15024.
38. Miyoshi, D., Karimata, H., and Sugimoto, N. (2006) Hydration regulates thermodynamics of G-quadruplex formation under molecular crowding conditions. *J. Am. Chem. Soc. 128*, 7957–7963.
39. Qi, J., and Shafer, R. H. (2007) Human telomere quadruplex: Refolding and selection of individual conformers via RNA/DNA chimeric editing. *Biochemistry 46*, 7599–7606.
40. Joachimi, A., Benz, A., and Hartig, J. S. (2009) A comparison of DNA and RNA quadruplex structures and stabilities. *Bioorg. Med. Chem. 17*, 6811–6815.
41. Randall, A., and Griffith, J. D. (2009) Structure of long telomeric RNA transcripts: The G-rich RNA forms a compact repeating structure containing G-quartets. *J. Biol. Chem. 284*, 13980–13986.
42. Olsen, C. M., and Marky, L. A. (2009) Energetic and hydration contributions of the removal of methyl groups from thymine to form uracil in G-quadruplexes. *J. Phys. Chem. B 113*, 9–11.
43. Olsen, C. M., Lee, H. T., and Marky, L. A. (2009) Unfolding thermodynamics of intramolecular G-quadruplexes: Base sequence contributions of the loops. *J. Phys. Chem. B 113*, 2587–2595.
44. Arora, A., and Maiti, S. (2009) Differential biophysical behavior of human telomeric RNA and DNA quadruplex. *J. Phys. Chem. B 113*, 10515–11520.
45. Richard, E. G. (1975) Handbook of Biochemistry and Molecular Biology, CRC Press, Cleveland, OH.
46. Goobes, R., Kahana, N., Cohen, O., and Minsky, A. (2003) Metabolic buffering exerted by macromolecular crowding on DNA-DNA interactions: Origin and physiological significance. *Biochemistry 42*, 2431–2440.
47. Xu, Y., Kaminaga, K., and Komiyama, M. (2008) G-quadruplex formation by human telomeric repeats containing RNA in Na^+ solution. *J. Am. Chem. Soc. 130*, 11179–11184.
48. Martadinata, H., and Phan, A. T. (2009) Structure of propeller-type parallel-stranded RNA G-quadruplexes, formed by human telomeric RNA sequences in K^+ solution. *J. Am. Chem. Soc. 131*, 2570–2578.
49. Danial, N. N., and Korsmeyer, S. J. (2004) Cell death. *Cell 116*, 205–219.
50. Negrini, M., Silini, E., Kozak, C., Tsujimoto, Y., and Croce, C. M. (1987) Molecular analysis of *mbcl*-2: Structure and expression of the murine gene homologous to the human gene involved in follicular lymphoma. *Cell 49*, 455–463.
51. Drew, H. R., Wing, R. M., Takano, T., Broka, C., Tanaka, S., Itakura, K., and Dickerson, R. E. (1981) Structure of a B-DNA dodecamer: Conformation and dynamics. *Proc. Natl. Acad. Sci. U.S. A. 78*, 2179–2183.
52. Sacca, B., Lacroix, L., and Mergny, J. L. (2005) The effect of chemical modifications on the thermal stability of different G-quadruplex-forming oligonucleotides. *Nucleic Acids Res. 33*, 1182–1192.
53. Nakano, S., Karimata, H., Ohmichi, T., Kawakami, J., and Sugimoto, N. (2004) The effect of molecular crowding with nucleotide length and cosolute structure on DNA duplex stability. *J. Am. Chem. Soc. 126*, 14330–14331.
54. Hall, K., Cruz, P., Tinoco, I., Jovin, T. M., and van de Sande, J. H. (1984) 'Z-RNA': A left-handed RNA double helix. *Nature 311*, 584–586.
55. Auffinger, P., and Westhof, E. (2001) Water and ion binding around $r(UpA)_{12}$ and $d(TpA)_{12}$ oligomers: Comparison with RNA and DNA $(CpG)_{12}$ duplexes. *J. Mol. Biol. 305*, 1057–1072.
56. Egli, M., Portmann, S., and Usman, N. (1996) RNA hydration: A detailed look. *Biochemistry 35*, 8489–8494.
57. Haider, S., Parkinson, G. N., and Neidle, S. (2002) Crystal structure of the potassium form of an *Oxytricha nova* G-quadruplex. *J. Mol. Biol. 320*, 189–200.
58. Pan, B., Shi, K., and Sundaralingam, M. (2006) Base-tetrad swapping results in dimerization of RNA quadruplexes: Implications for formation of the i-motif RNA octaplex. *Proc. Natl. Acad. Sci. U.S.A. 103*, 3130–3134.